Hindawi
International Journal of Photoenergy
Volume 2022, Article ID 5136887, 15 pages
https://doi.org/10.1155/2022/5136887

Research Article

Design and Implementation of a New Fast and Efficient MPPT Controller under Different Solar Irradiance Conditions

K. Padmanaban,[1] **A. Shunmugalatha**,[2] **and M. S. Kamalesh**[3]

[1]*Department of Electrical and Electronics Engineering, Alagappa Chettiar Government College of Engineering and Technology, Karaikudi, 630003 Tamil Nadu, India*
[2]*Department of Electrical and Electronics Engineering, Velammal College of Engineering and Technology, Madurai, 625009 Tamil Nadu, India*
[3]*Department of Electrical and Electronics Engineering, Kongu Engineering College, Erode, 638060 Tamil Nadu, India*

Correspondence should be addressed to K. Padmanaban; kpadmanaban@accetedu.in

Received 16 May 2022; Revised 8 November 2022; Accepted 17 November 2022; Published 21 December 2022

Academic Editor: Regina De Fátima Peralta Muniz Moreira

The power-voltage (P-V) characteristic curve of solar photovoltaic (PV) systems operating in partial shading conditions (PSC) is nonlinear and has multiple local maximum peak power (LMPP) points, rendering many of the maximum power point tracking (MPPT) algorithms ineffective at locating global maximum peak power (GMPP) points. This work proposes a novel slime mould algorithm- (SMA-) based MPPT controller to utilise maximum peak power (MPP) from solar PV systems during uniform irradiance conditions (UC) and nonuniform irradiance conditions (NUC). On the basis of the MPP they tracked, tracking time, and power efficiency, MPPT controller performance is assessed through MATLAB simulations and implemented experimentally with dSPACE MicroLabBox under various irradiance conditions. The effective performance of the proposed controller is validated and demonstrated in comparison to existing popular MPPT controllers.

1. Introduction

The need for increased power generation capacity today is unavoidable, and the majority of research are concentrating on renewable energy sources due to their infinite nature and little emissions [1]. Solar panels have the highest energy density of any energy source, making them the most cost-effective option today compared to thermal and vibration sources [2]. The main problem with using solar PV systems is the strong nonlinearity between power and voltage. Fluctuations in solar irradiation and temperature lower the PV array's overall maximum power delivery capacity [3]. MPPT is required to track the MPP of PV arrays in solar renewable energy systems (SRES) because solar PV systems are not a constant source of electric power [4]. PV arrays are made up of PV panels that are connected in series for high voltage and parallelly connected for high current applications, respectively, to increase the PV array power. Blocking and bypassing diodes are important for efficient performance in solar PV systems. Backward discharge is avoided by blocking diodes. Bypass diodes minimize power loss caused by PSC and prevent hotspot heating [5]. The PSC occurs due to nonhomogeneous solar irradiation over the PV array due to a tree or building shading, dust, and bird droppings. Besides, PSC produces several peaks in P-V characteristics and power losses. To lessen power loss caused by PSC, numerous MPPT techniques have been developed and used [6].

The effectiveness of various MPPT approaches is analysed based on how accurately and instantaneously they track maximum power on different PSCs. Based on their tracking capabilities, the available MPPT methods are categorized into three types: classical MPPT controllers, intelligent MPPT controllers, and optimization MPPT

controllers [7]. The perturb and observe (PO), incremental conductance (IC), open circuit voltage (OCV), short circuit current (SCC), and hill-climbing method (HC) are examples of traditional MPPT controllers. Traditional controllers are popular for their easy and affordable implementation, but they are frequently inaccurate since they may miss the global peak during PSC in favour of a local peak; also, there will be steady-state oscillation around MPP [8]. Artificial neural networks, sliding mode, fuzzy logic-based controllers, and golden ratio-based controllers are a few of the most well-known intelligent MPPT controllers [9]. Although intelligent MPPT controllers are quick and effective, each has its drawbacks. For example, ANNs require a lot of data to train the system, which drives up the cost of the controller. FLCs are also more affordable, but their implementation complexity is higher due to challenging membership function tuning, rule matrix formation, scaling factor, and operation range selection. The choice of sliding surface affects SMC performance [10].

Some popular optimization-based MPPT controllers include particle swarm optimization (PSO) [11], cuckoo search optimization (CS) [12], ant colony optimization algorithm (ACO) [13], genetic algorithm (GA) [14], grey wolf optimization (GWO) [15], ant bee colony optimization (ABC) [16], and salp swarm optimization (SSA) [17]. PSO and GA have the ability to track MPP but with the drawback of steady-state oscillation. ACO, SSO, and GA have the drawback of high complexity in implementation. CS can track MPP accurately but with a very low convergence speed, and also, it needs periodic tuning throughout the operation. GWO and ABC have the demerit of high computational time, cost, and complexity due to their large search space. Along with the aforementioned shortcomings, the controllers outlined above are vulnerable to becoming stuck in LMPP because of their laborious search technique toward the global optimum. In addition to the aforementioned drawbacks, the controllers described above are susceptible to getting stuck in LMPP due to their monotonous search strategy for the global optimum.

The SMA [18], a newly developed stochastic optimizer based on the biooscillation characteristics of slime mould (SM). The SMA-based MPPT controller can dynamically change its search strategy according to the fitness of the current solution (food) it achieves. The proposed controller leaves the solution and begins exploring the food sources with high exploration capability if the current solution fitness is low. If the current solution fitness is high, the SMA-based controller uses a region-limited search strategy with high exploitation capability around that specific solution. The SMA-based MPPT controller locates GMPP using this adaptive searching technique, preventing it from becoming caught in LMPP.

To modify the PV output current's unfavourable characteristics, a DC-DC converter is required [19]. A DC-DC converter is required to improve system reliability and efficiency [20]. Traditional converters used in solar PV systems include boost [21], single-ended primary inductance converter (SEPIC) [22], ZETA [23], and Cuk converter [24]. The influence of irradiance along with temperature fluctuations in a PV system designing has been explored by Farahat et al. [25], and they discovered that buck-boost and Cuk converter could give the best output power without taking the load value into account. According to Taghvaee et al. [26], buck-boost, Cuk, and SEPIC converters offer the best tracking performance for PV applications since they are not affected by atmospheric conditions. The Cuk converter worked well because of the subtle difference in ripples existing in the circuit.

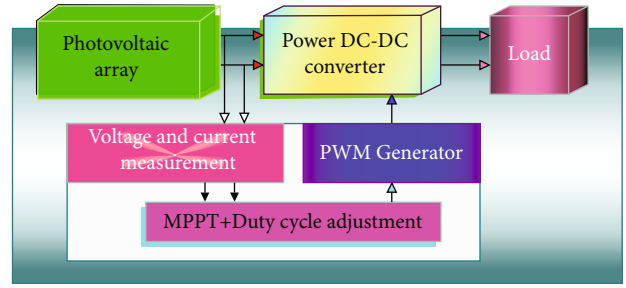

Figure 1: Block diagram of solar PV system.

The block diagram of a solar PV system with SMA-based MPPT controller is shown in Figure 1. The Cuk converter converts the energy from the solar panel to the load. The Cuk converter regulates solar panel voltage and current to control PV power. Due to their fluctuation in response to solar irradiation and temperature, the SMA-MPPT controller continuously modifies the duty cycle.

The primary goal of the research project is to develop an effective MPPT method that uses a PV system with a Cuk converter based on the SMA algorithm.

(i) Under varying climatic circumstances, it can track the maximum power and deliver continuous output using a Cuk converter

(ii) To increase reliability, it has a high convergence speed and restricts computational complexity

(iii) The proposed system has excellent dynamic performance, has no steady-state oscillation, and can track the MPP effectively

The rest of the paper is organized as follows: the SM method is discussed in Section 2, and Section 3 proposes the SMA algorithm for MPPT with the Cuk converter. Testing the proposed methods under nonuniform atmospheric conditions yields the simulation results of the SMA-MPPT with the Cuk converter that are described in Section 4. The experimental outcomes are presented in Section 5, and finally, conclusions are reached in Section 6.

2. Slime Mould Optimization Algorithm

A unique metaheuristic algorithm called the SM method was introduced by Li et al. in 2020, to provide a more flexible and effective method. The SMA method is a contemporary metaheuristic algorithm that was developed after researching the SMA in nature. Few parameters, robustness, and strong

```
Initialize the parameters population size and termination criteria
Initialize the positions of Individual slime, X_i(i = 1, 2, ⋯, n);
while (t ≤ Max_t)
        Calculate the fitness of all search agents
        Update best fitness value, X_b
        Calculate W
        for each search
                Update p, vb, vc;
                Update population positions
        end for
        t = t + 1;
end while
return best fitness, X_b
```

Algorithm 1: Pseudocode of SMA.

exploratory and exploitation capability are only a few of its features.

The SMA algorithm incorporates the ideal meal path of positive and negative feedback mechanism. Based on the availability of the nutrients, SM instantly alter their search patterns. The three basic elements of the SMA method are the grabble, approach, and wrap phenomena. When trying to find food, the grabble phenomenon prevents search agents from clashing. Slime mould velocity matching is demonstrated via the wrap phenomena. Furthermore, the approach phenomenon makes the SM learn about the feeding centre. When different solutions have different qualities, SM might select the one with the highest fitness value. The mould evaluates the speed concerning the amount of food and the environmental risk. SM forages use empirical methods based on the limited data currently available to determine whether to begin a new search and move on from the previous place. Even if there is a plentiful supply, mould may divide its biomass to use various resources based on the knowledge of some expensive, high-quality foods. Depending on the quality of the food supply, it can change their search patterns on the fly.

The SMA method begins with a randomly generated search agents, where "N" represents the population size and "dim" represents the problem dimension. After that, fitness of the population has to be calculated. The search agent is updated in each iteration by grabbling, wrapping, and approaching techniques. Furthermore, several parameters, such as the fitness weight (W) of the individual, control the SMA algorithm's evolution, allowing for fast convergence. The vibration parameter (vb) enables the precision of each SM.

2.1. Approach food. Based on the fragrance in the air, the SM can approach food. The following equations are given to simulate the approaching behavior of contraction mode.

$$\overrightarrow{X(t+1)} = \begin{cases} \overrightarrow{X_b(t)} + \overrightarrow{\mathrm{vb}} * \left(\vec{W} * \overrightarrow{X_A(t)} - \overrightarrow{X_B(t)}\right), & r < p, \\ \overrightarrow{\mathrm{vc}} * \overrightarrow{X(t)}, & r \geq p. \end{cases} \tag{1}$$

where $\overrightarrow{\mathrm{vb}}$ and $\overrightarrow{\mathrm{vc}}$ are the adjustable parameters, X_b is the location of each particle in the zone where odour is greatest, X is the location of the mould, X_A and X_B are the randomly picked variables from the SM, and W is the SM weight.

The following is the maximum limit of p:

$$p = \tanh |S(i) - DF|, \text{ where i} \in 1, 2, \cdots..n, \tag{2}$$

where S(i) ranks the population, while DF reflects the greatest fitness gained in all iterations.

The vibration parameter is defined by

$$\overrightarrow{\mathrm{v}b} = [-\mathrm{a}, \mathrm{a}], \tag{3}$$

$$\mathrm{a} = \operatorname{arctanh}\left(-\left(\frac{t}{\mathrm{Max}_t}\right) + 1\right). \tag{4}$$

The slime mould weight represented by

$$\overrightarrow{W\left(\text{smell index}\left(i\right)\right)} = \begin{cases} 1 + r * \log\left(\dfrac{\mathrm{bF} - S(i)}{\mathrm{bF} - \mathrm{wF}} + 1\right), & \text{condition}, \\ 1 - r * \log\left(\dfrac{\mathrm{bF} - S(i)}{\mathrm{bF} - \mathrm{wF}} + 1\right), & \text{others}, \end{cases} \tag{5}$$

where r signifies [0, 1], bF is the optimal value of fitness in the current iteration, and wF is the worst fitness in the current iteration.

The fitness weight W and the vibration parameter vb balance exploration and exploitation. Smell index specifies the sequence of fitness values, as specified by

$$\text{Smell index} = \text{sort}\left(S\right). \tag{6}$$

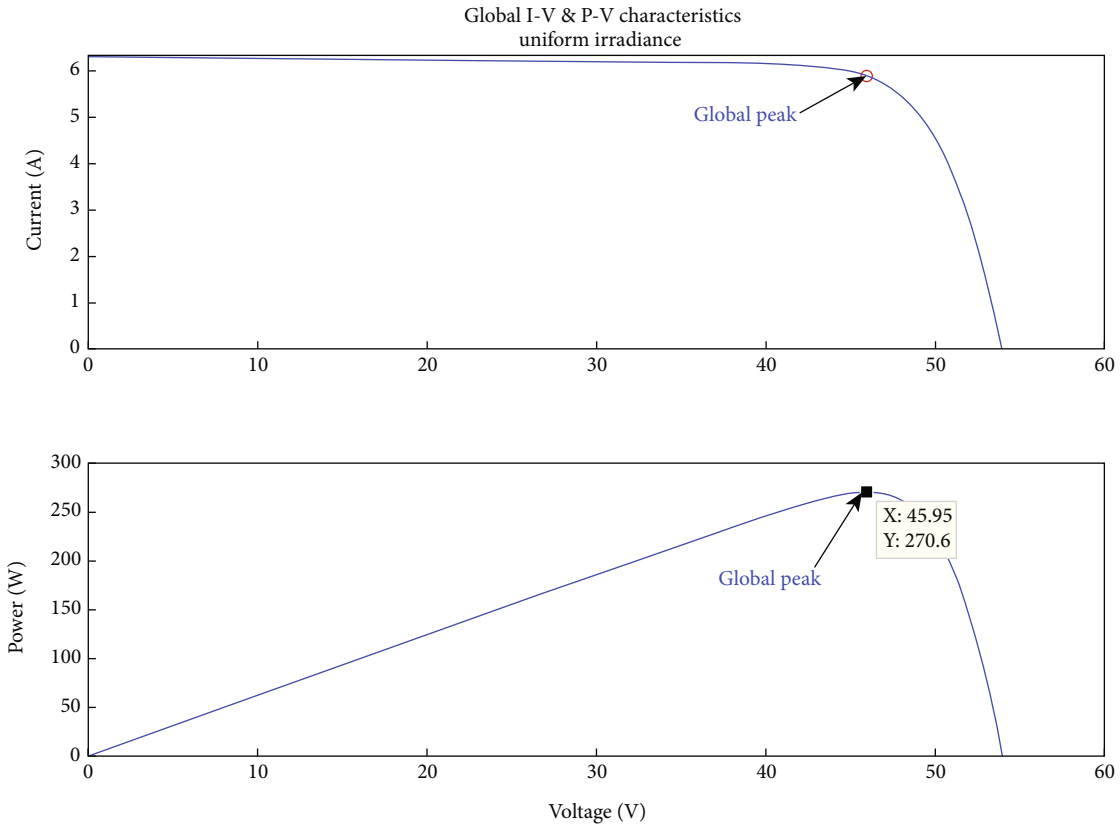

(a)

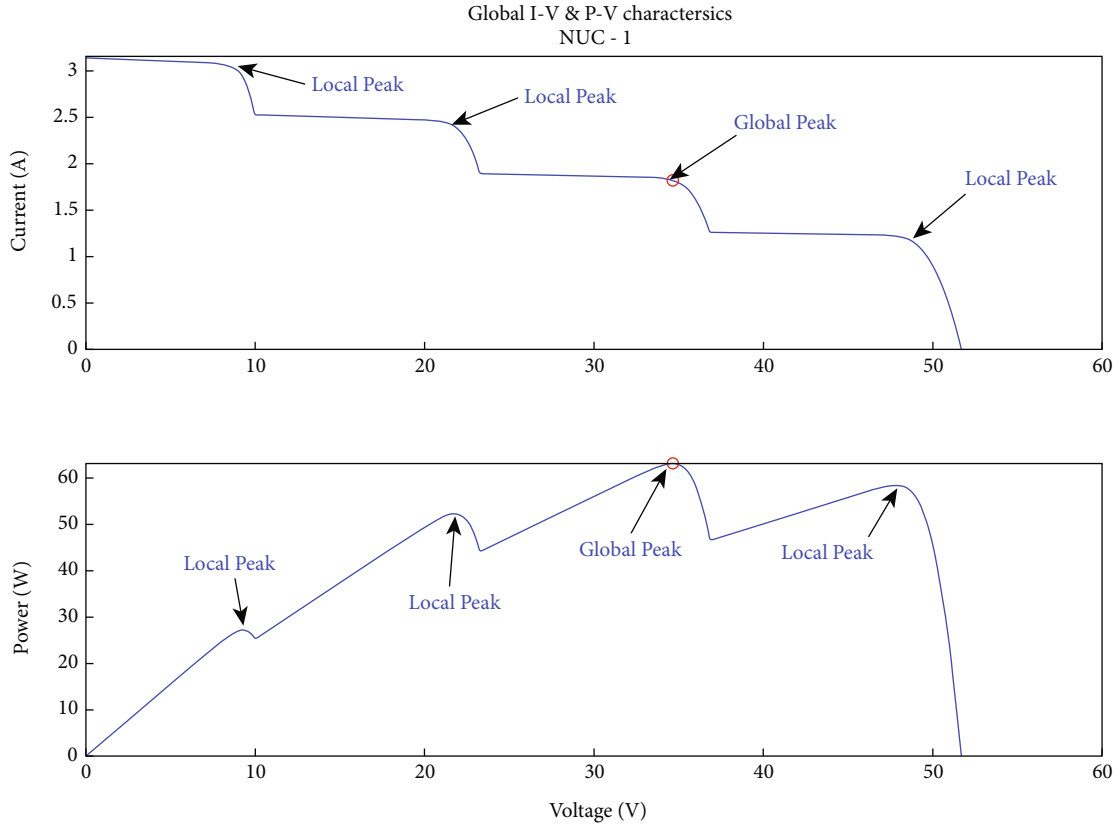

(b)

Figure 2: Continued.

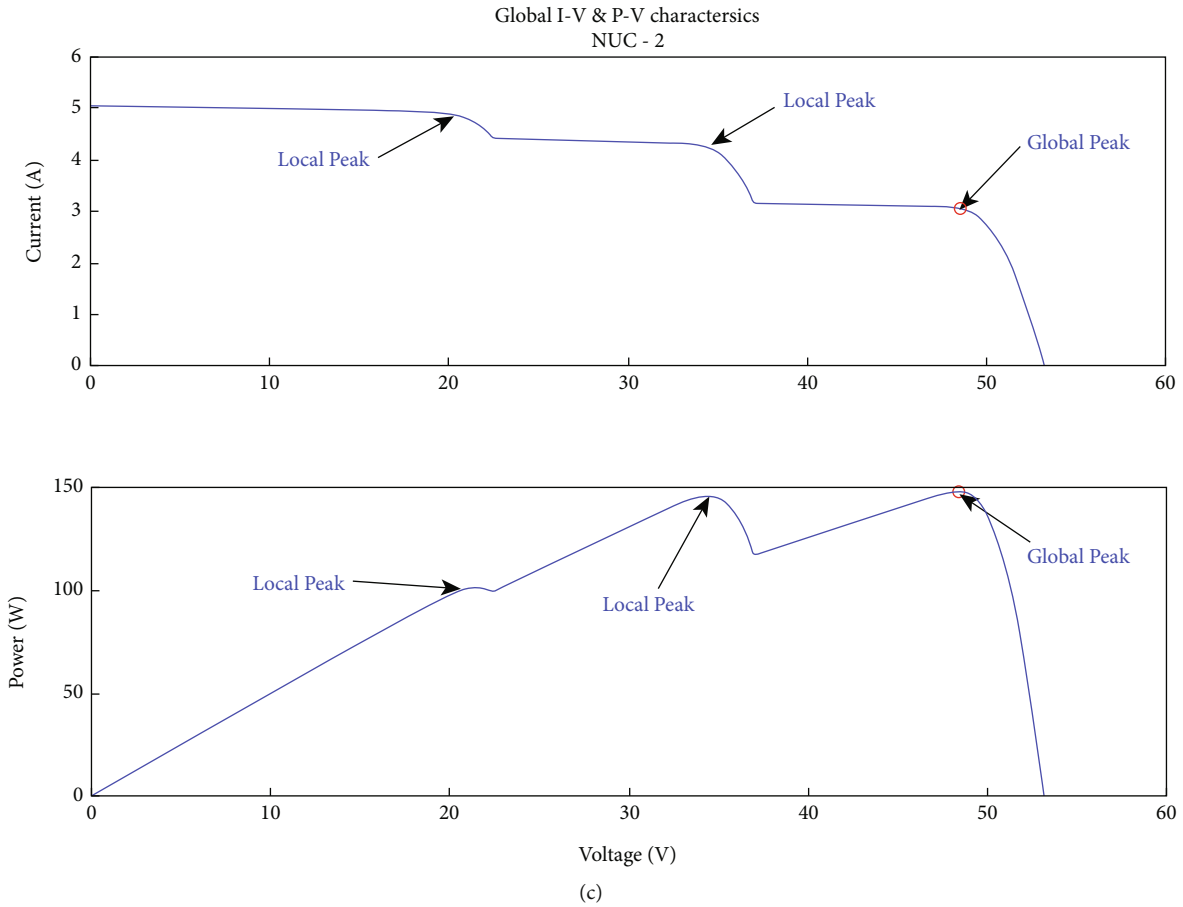

FIGURE 2: (a) Nonlinear I-V and P-V curve characteristics of PV panel at uniform conditions (1000 W/m^2). (b) Nonlinear I-V and P-V curve characteristics of PV panel at nonuniform conditions-1 (300, 400, 200, and 500 W/m^2). (c) Nonlinear I-V and P-V curve characteristics of PV panel at nonuniform conditions-2 (500, 800, 700, and 800 W/m).

According to equation (1), individual X is updated with best position X_b currently attained, and the location of the individual can be changed by fine-tuning the parameters vb, vc, and W. Individuals can build search trajectories at any angle, i.e., explore key space in any path, by picking two random variables from SM. This permits the algorithm to discover the finest solution. Thus, it allows persons searching for an optimal solution to search in all available directions, imitating the circular shape of SM while approaching food. Extending this notion to hyperdimensional space is also possible.

According to equation (5), the positive and negative feedback of the individual search agent and the food content has been investigated. Meanwhile, the component r represents the uncertainty of the shrinkage mode. The log has been used to slow down the rate at which numerical values change, allowing the shrinkage frequency value to remain stable.

2.2. Wrap food. When the food quality is high, the weight near the food is greater; when the food quality is low, the weight is lowered, and the focus shifts to other areas to be explored. The mathematical expression for updating the position of SM, i.e., to wrap the food, is given in equation (7), based on the principle.

$$\overrightarrow{X^*} = \begin{cases} \text{rand} * (UB - LB) + LB, & \text{rand} < z, \\ \overrightarrow{X_b(t)} + \overrightarrow{\text{vb}} * \left(\vec{W} * \overrightarrow{X_A(t)} - \overrightarrow{X_B(t)}\right), & r < p, \\ \overrightarrow{\text{vc}} * \overrightarrow{X(t)}, & r \geq p. \end{cases} \tag{7}$$

2.3. Grab food. As the repetitions increases, the vb oscillates arbitrarily within $[-a, a]$ and goes to zero. The value of vc oscillates within $[-1, 1]$ and finally goes to zero. Furthermore, vb indicates the state of population determining whether to approach the food source or seek for additional food sources through its oscillation mechanism. The pseudocode of the SMA is given in Algorithm 1.

3. Proposed SMA-MPPT with Cuk Converter

Due to irregular availability, PV deployments face numerous difficulties. As illustrated in Figure 2, the PV array's output curves, which include current-voltage (I-V) and P-V characteristics, are nonlinear and divided into three categories. Short circuit current (I_{sc}) is the highest current

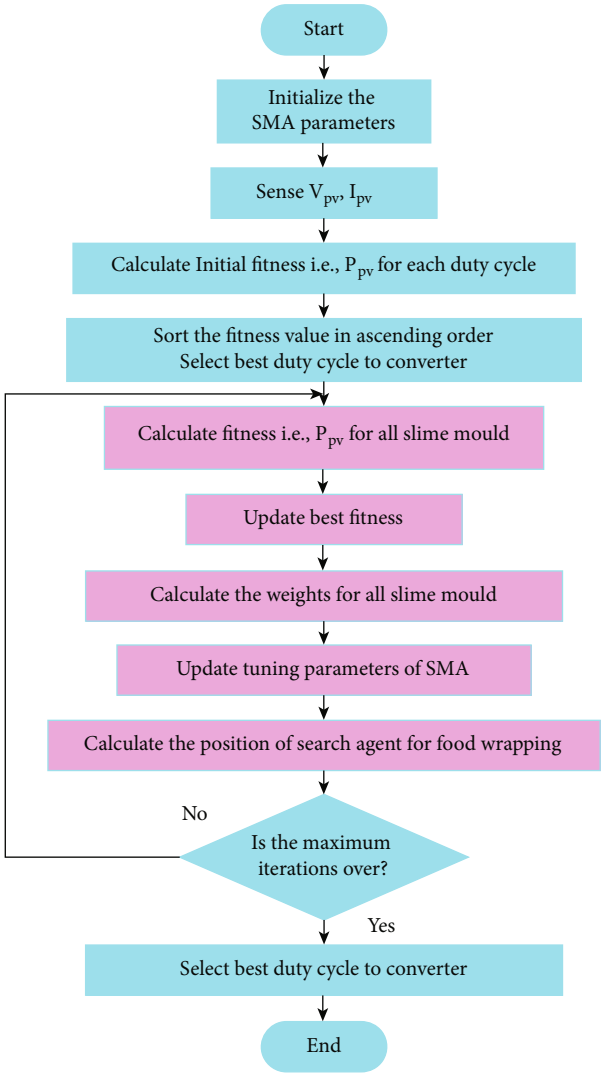

Figure 3: Flowchart of SMA-MPPT algorithm.

(I_{max}), whereas open-circuit voltage (V_{oc}) is the highest voltage (V_{max}).

Tracking the MPP, which is the product of voltage at MPP(V_{mpp}) and current at MPP (I_{mpp}) at the MPP, can boost efficiency in comparison to a system without MPPT by 30%.

Many MPPT research articles concentrate on cutting tracking time and improving MPPT effectiveness. This leads to a technological saturation when attempting to determine MPP for a given voltage and current under uniform conditions (UC), that is, when the irradiation is 1000 W/m^2 and the temperature is 25°C as illustrated in Figure 2(a). However, as shown in Figures 2(b) and 2(c), under PSC, the operating curves have several peaks on the P-V curve and I-V curve. This necessitates a very difficult and exceptional method to determine the appropriate duty cycle for generating the GMPP. The majority of MPPT approaches are caught by the several LMPPs that make up the numerous peaks.

The proposed MPPT controller's step-by-step operation is clearly explained in Figure 3, the flowchart of the SMA-

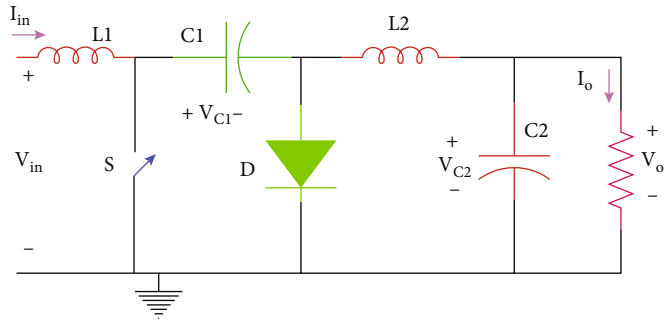

Figure 4: Circuit diagram of Cuk converter.

Table 1: Parameters of the Cuk converter.

Parameters	Values
Switching frequency (fs)	50 KHz
Circuit inductor (L_1)	1.1478 mH
Circuit inductor (L_2)	1.478 mH
Circuit capacitor (C_1)	0.5 mF
Circuit capacitor (C_2)	0.5 mF
Resistive load (R)	50 ohm

MPPT controller. The controller determines the power generated after initializing the SMA parameters and receiving data from sensors monitoring the terminal V and I of solar PV arrays. The controller then assigns each search agent in the population a random and unique duty cycle. Fitness values are assigned for each SM by calculating the PV power corresponding to that duty cycle. The SM location with the high fitness value is saved as GMPP. To imitate the behavior of a biooscillatory nature of using its positive and negative feedback to select the best food source depending on the feeding vein thickness, it is crucial to calculate the weights for each SM. This weight-based search method speeds up the algorithm and keeps it from getting stuck in an LMPP with high exploration capability. As the position of the GMPP may shift and the solar irradiation changes continuously, PSC may happen at any time. Therefore, periodic tuning of the parameters is needed to alter the location of each slime. Thereafter, the process of determining each individual's fitness is repeated until the termination criterion is satisfied.

Due to the advantages, such as few control parameters, robustness, great exploratory capability, and inclination exploitation, the SMA is capable of exploring better solution for complex problems. The optimal operation of PV based on the SMA for MPP tracking under NUC is solved for the first time in this paper. A new intelligent SMA algorithm capable of finding the GMPP and guaranteeing maximum power transfer is proposed. This SMA-MPPT method is used to control a PV arrangement comprised of four 100 W PV modules.

The DC-DC converter is the main component of the solar PV system; the duty ratio associated with the MPP is calculated by comparing the MPPT method's gate pulses across the switch to the converter's switching frequency. When developing an MPPT technique, the vital concern is

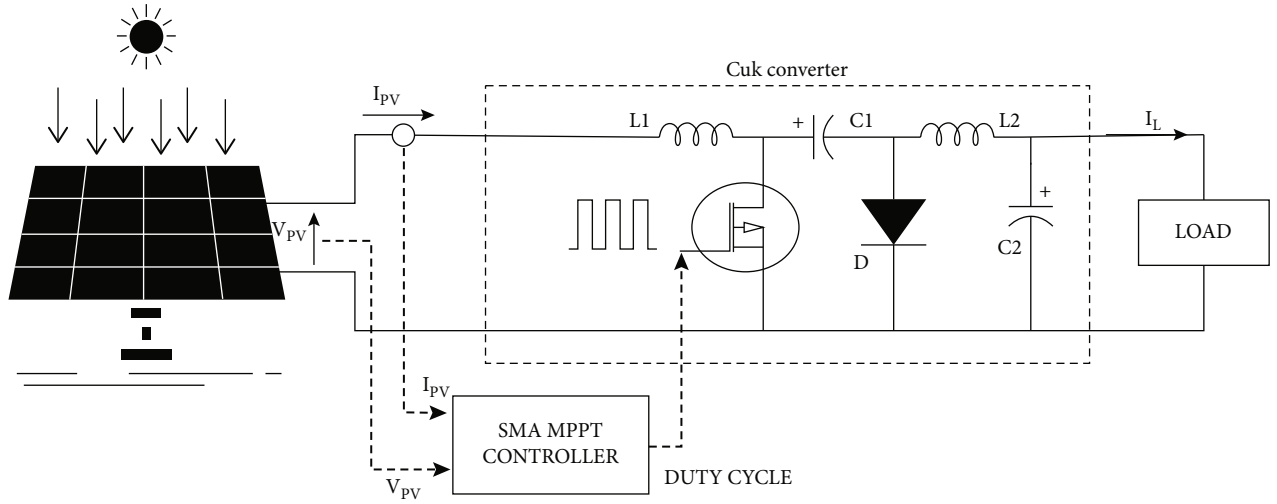

Figure 5: Solar PV system with SMA-MPPT controller using Cuk converter.

to choose and construct an efficient converter that will serve as the MPPT system's core component.

The switched-mode DC-DC converters has received a lot of attention. Cuk converter offers the lowest switching losses and the maximum efficiency compared with other nonisolated DC-DC converters. The equivalent circuit of Cuk converter is shown in Figure 4. The Cuk converter operates in the continuous conduction mode. Two inductors (L_1 and L_2), two capacitors (C_1 and C_2), a switch (S), a diode (D), and resistive load (R) are the essential components of the Cuk converter.

The Cuk converter's voltage transfer function is given by

$$\frac{V_o}{V_{\text{in}}} = \frac{D}{1-D}, \tag{8}$$

where D is duty cycle and the inductor's ripple current are approximately equal. To build a Cuk converter to a particular specification, the equations (9)–(12) have been used to choose the design parameters of the Cuk converter.

$$L_1 = \frac{V_{\text{in}} * D}{f_s * \Delta I_{L1}}, \tag{9}$$

$$L_2 = \frac{V_{\text{in}} * D}{f_s * \Delta I_{L2}}, \tag{10}$$

$$C_1 = \frac{V_o * D}{f_s * \Delta V_{C1} * R}, \tag{11}$$

$$C_2 = \frac{V_o * (1-D)}{f_s^{\,2} * \Delta V_o * 8 * L_1}, \tag{12}$$

where f_s is the switching frequency, ΔI_{L1} and ΔI_{L2} are the ripple current of inductors L_1 and L_2, respectively, ΔV_{C1} is the ripple voltage across capacitor C_1, and ΔV_o is the output voltage ripple.

Table 2: Specifications of PV module.

Parameters	Values
Short circuit current (I_{sc})	6.71 A
Open circuit voltage (V_{oc})	20.20 V
Current at MPP (I_{mpp})	6.07A
Voltage at MPP (V_{mpp})	16.70 V
Maximum power (P_{max})	101.30 W
Current temperature coefficient	-0.379%/°C
Voltage temperature coefficient	0.039%/°C

The Cuk converter is perfect for MPPT applications because it is radiation and temperature independent, allowing it to follow the maximum point. The parameters of the Cuk converter are specified in Table 1.

4. Simulation Results and Discussion

The MATLAB/Simulink tool is used to examine the proposed solar PV system's dynamic characteristics under various meteorological conditions. Figure 5 depicts the system, which includes a PV array, MPPT algorithm, and Cuk converter. To boost the PV output voltage, the PV array consists of four modules connected in series. Table 2 gives the specifications of PV module used in simulation.

As seen in Figure 5, the MPPT algorithm and Cuk converter assist in extracting MPP from a solar PV arrangement. The output power of the PV is directly related to the received solar irradiation and inversely related to temperature. At constant temperature, this leads to a net gain in PV output power with increased insolation.

Every PV cell has unique maximum output power at a specific light intensity, which is known as the MPP. The power output of a PV module differs with operational temperature and light intensity, based on the simulation results. When the atmospheric condition changes, the MPP varies as

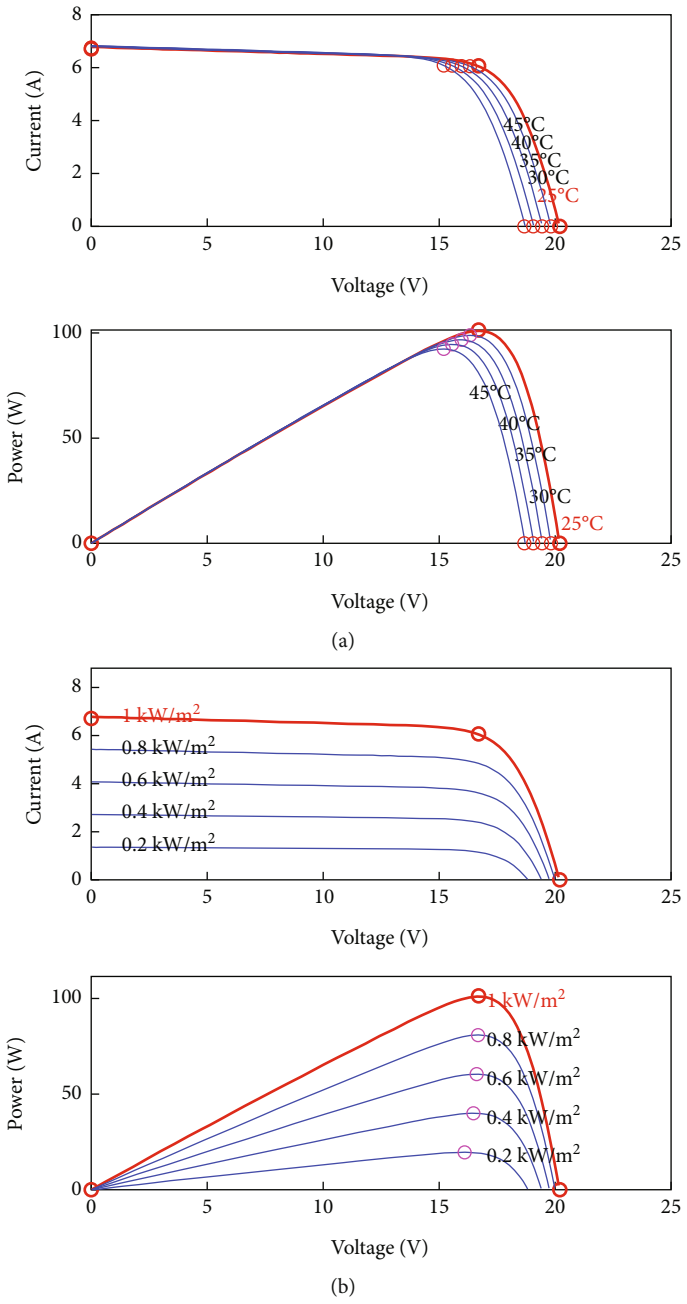

Figure 6: (a) Characteristics of PV module with the effect of temperature variations. (b) Characteristics of PV module with the effect of insolation variations.

well. When this occurs, the MPP must be traced by varying array terminal voltage with a Cuk converter.

As demonstrated in Figure 6(a), the PV output power is inversely related to temperature and directly related to the amount of solar energy received. The P-V and I-V curves of a PV array under constant temperature and varying insolation conditions are shown in Figure 6(b). As insolation rises, the PV module's output current and voltage increase. This results in a net increase in PV output power with increased insolation at a constant temperature. The MPP, or maximum power point, is a unique maximum output power for photovoltaic cells at a particular light intensity. According to the results of the simulation, a PV module's output power varies with operational temperature and light intensity.

As the output power is restricted for individual solar PV panels, interconnection of solar PV panels into PV array is necessary to increase power. Blocking diodes (series) and bypass diodes (parallel) are used to protect the PV array from the current reversal problem and hotspot issue, respectively. To signify the necessity of an MPPT controller, multiple peaks in the P-V characteristic curve are created for

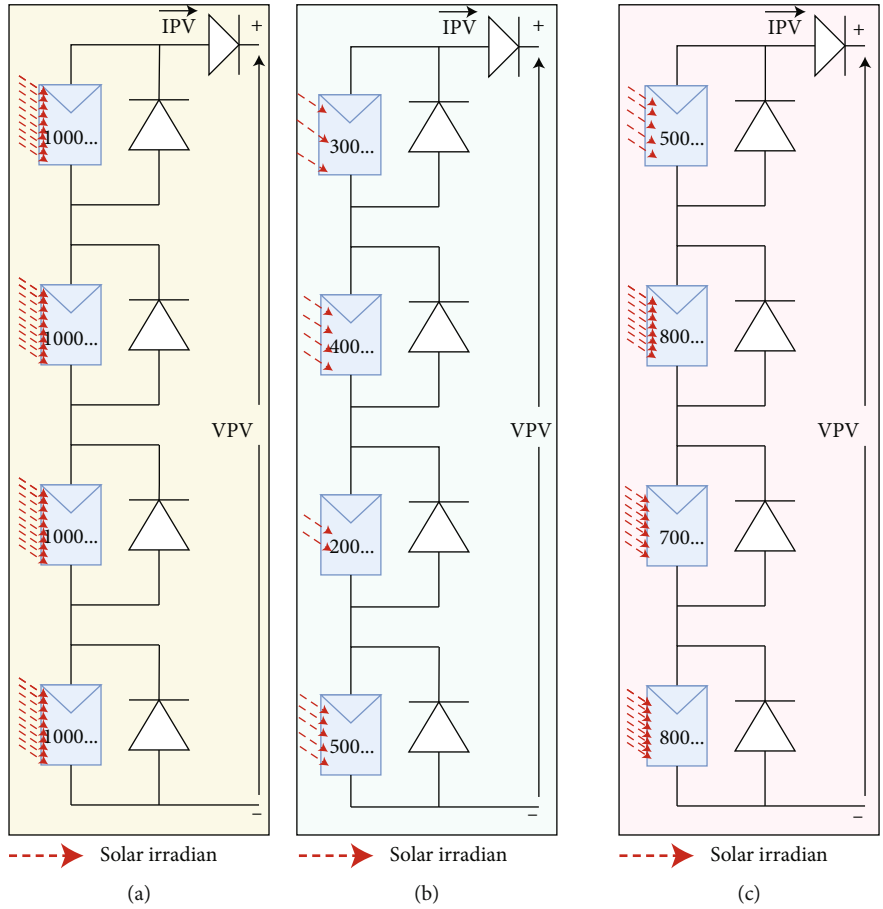

Figure 7: PV patterns on 4S configuration.

Table 3: Shade profile and GMPP for 4S PV configuration.

Solar PV configuration	Irradiance condition	Shade profile	Number of peaks in I-V and P-V curve	Global maximum peak power
4S	Uniform irradiance condition	Panel 1 = 1000 W/m^2 Panel 2 = 1000 W/m^2 Panel 3 = 1000 W/m^2 Panel 4 = 1000 W/m^2	1	270.60 W
	Nonuniform irradiance condition-1	Panel 1 = 300 W/m^2 Panel 2 = 400 W/m^2 Panel 3 = 200 W/m^2 Panel 4 = 500 W/m^2	4	62.15 W
	Nonuniform irradiance condition-2	Panel 1 = 500 W/m^2 Panel 2 = 800 W/m^2 Panel 3 = 700 W/m^2 Panel 4 = 800 W/m^2	3	149.91 W

4S (4 PV panels in series) configuration. Using 3 various solar irradiance patterns, LMPP and GMPP are created to test the performance of MPPT algorithms under complex conditions like PSC. As shown in Figure 7(a), all four panels are getting equal solar irradiance which is indicated by an equal number of red-dotted arrows, which is a uniform irradiance condition (UC). Figure 7(b) shows nonuniform irradiance condition (NUC-1), where all four panels are getting different solar irradiance levels, which is indicated with the help of the number of red-dotted arrows varied in direct proportion to the solar irradiance level, that particular panel is exposed to. In the same manner, Figure 7(c) indicates another case of nonuniform irradiance condition (NUC-2). Table 3 shows detailed description of all three solar

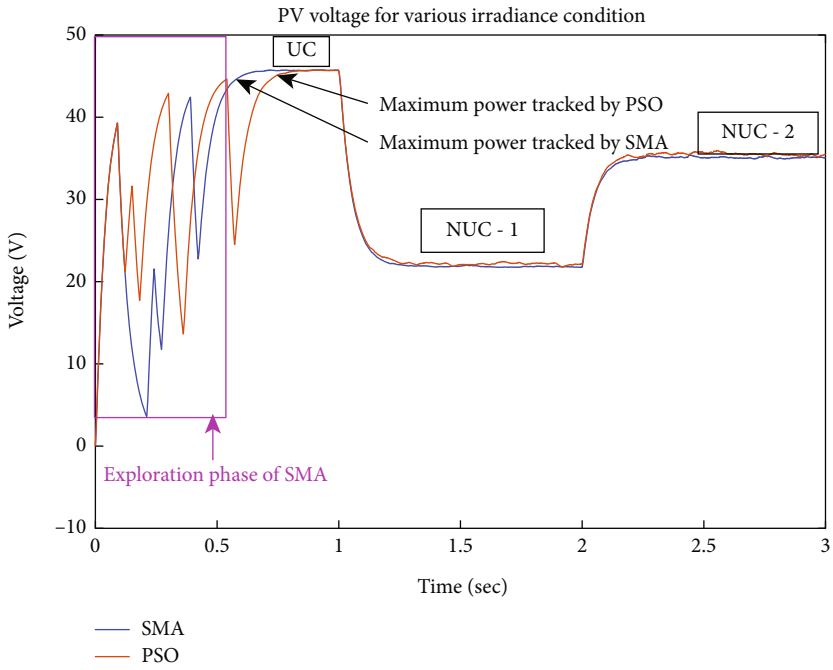

Figure 8: Convergence comparison of maximum power point based on PV voltage.

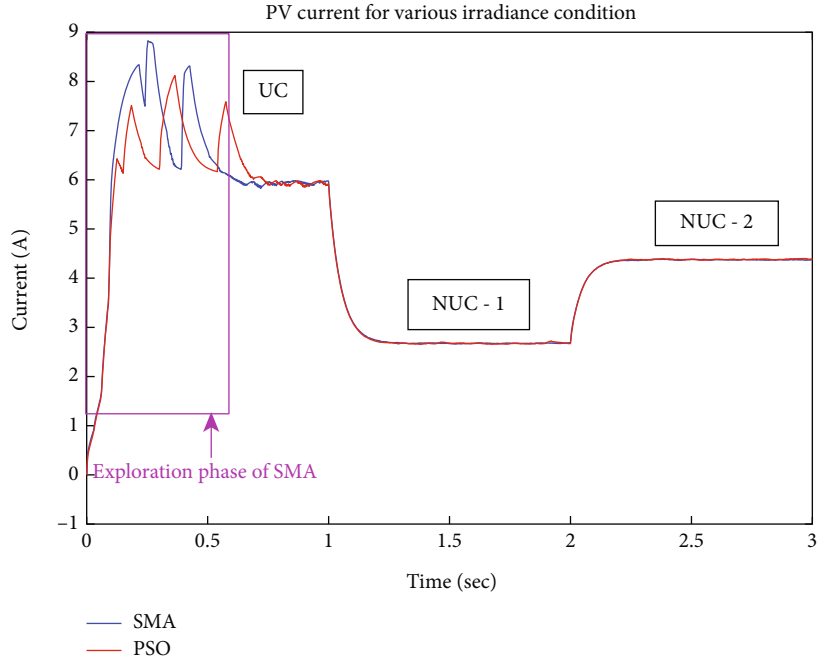

Figure 9: Convergence comparison of MPP based on PV current.

irradiance conditions considered for the study with corresponding GMPP.

The proposed SMA-MPPT algorithm with the Cuk converter has been verified for 4S configuration under both partially shaded situations and fast-changing irradiance conditions. The MPPT method is verified under two different nonuniform conditions (NUC) in PSC. The simulation platform for MATLAB was used to validate both. The duty cycle of the Cuk converter serves as the SM in the proposed SMA-MPPT algorithm. In the simulation of the PSO-MPPT method, the values for $C1$ and $C2$ are 1.4 and 1.8, respectively. During iteration, a fresh duty cycle is computed and used by the PWM controller. The output of the converter shifts as a result, and the transient reaction

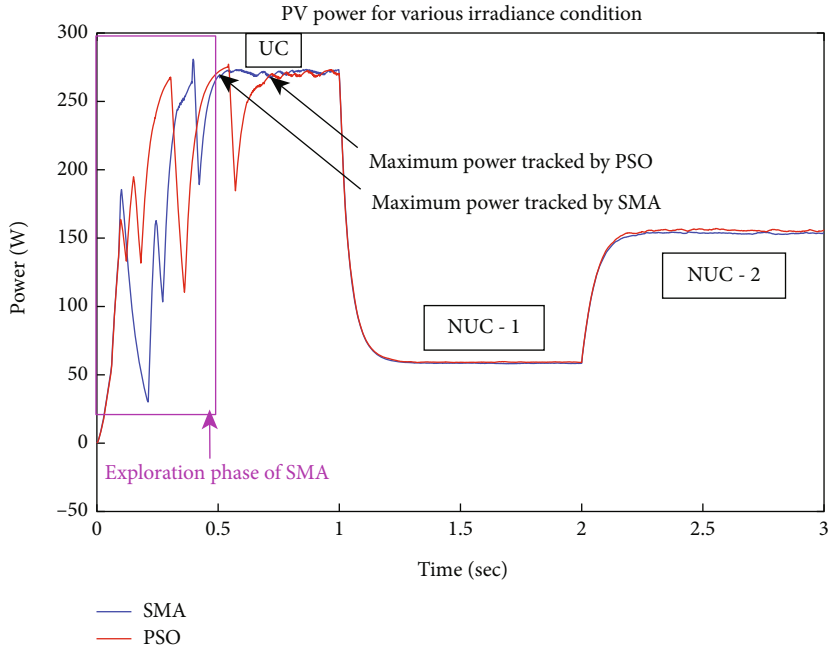

Figure 10: Convergence comparison of MPP based on PV power.

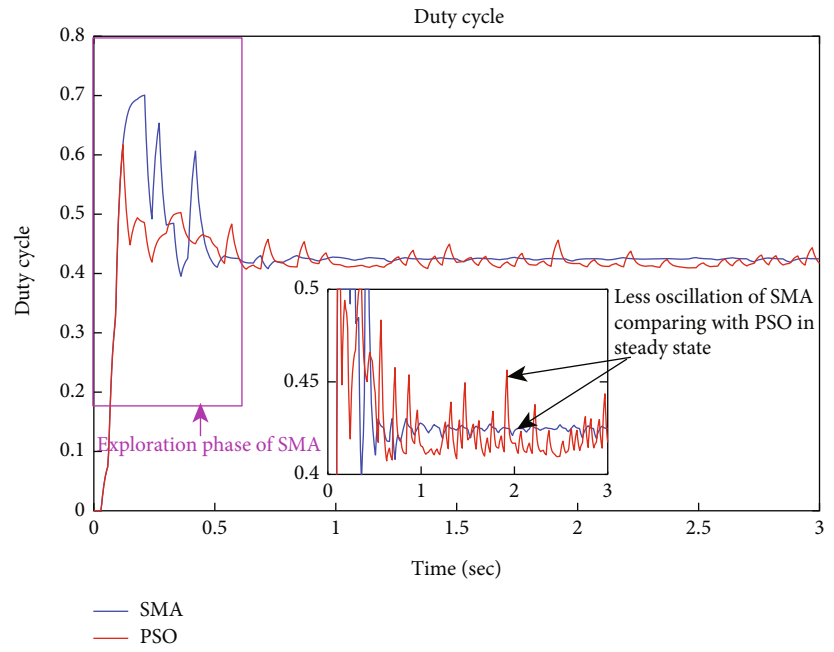

Figure 11: Convergence comparison of maximum power point based on duty cycle.

time the amount of time it takes to stabilize becomes longer. Consequently, the voltage and current sample durations should be longer than the PV system's sample time period.

The suggested MPPT method is compared to the PSO-MPPT algorithm to analyse the tracking time. The simulation results and hardware results are studied based on three irradiance conditions. (a) Uniform irradiance condition (1000 W/m^2), (b) (NUC-1) nonuniform irradiance condition-1 (300, 400, 200, and 500 W/m^2), and (c) (NUC-2) nonuniform irradiance condition-2 (500, 800, 700, and 800 W/m^2).

It is evident from Figure 8 that under uniform irradiance conditions, the maximum power point is 270.6 W with a maximum power voltage of 45.95 V. Figures 8–11 display the simulation results for all three situations.

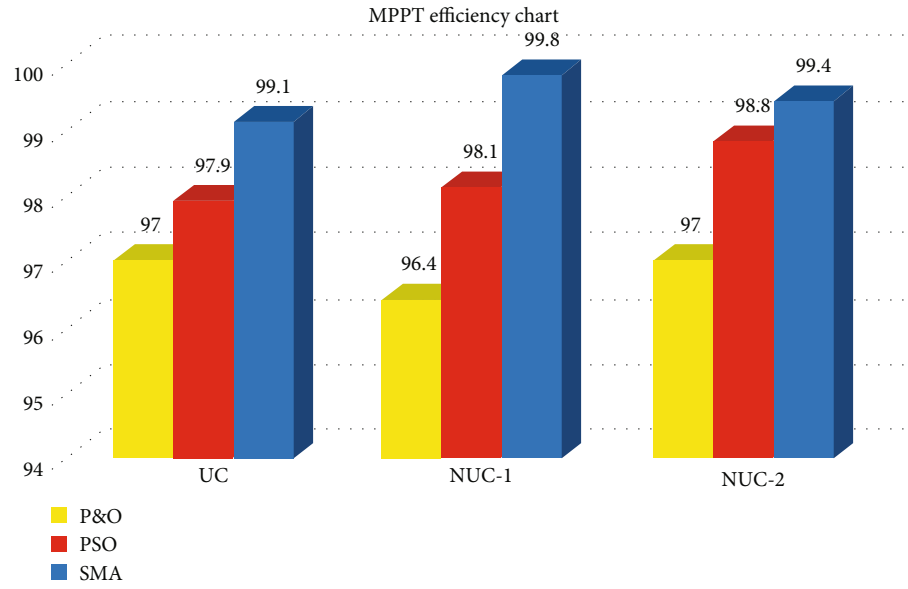

Figure 12: Comparison of the MPPT efficiency.

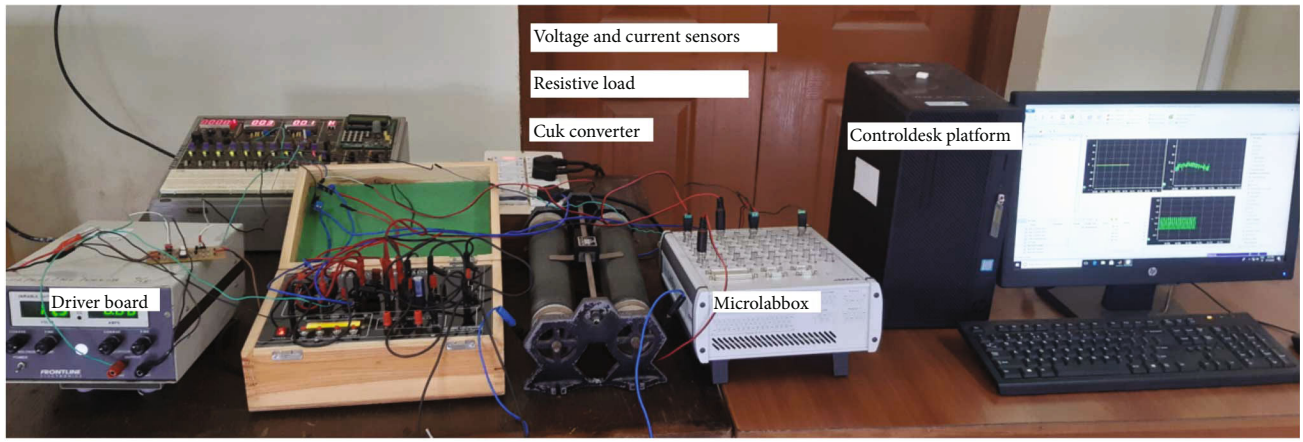

Figure 13: Hardware implementation of SMA-MPPT algorithm with Cuk converter using MicroLabBox.

Figure 8 illustrates how the proposed SMA-MPPT controller identifies MPP in 0.53 seconds as compared to 0.72 seconds for the PSO-MPPT controller. Consequently, the proposed algorithm tracks more efficiently than the PSO-MPPT algorithm. Any MPPT controller's tracking speed, which is the amount of time the algorithm needs to travel from its starting location to the point at which power fluctuation falls below 5%, is a key performance measure. Additionally, Figure 11 shows that SMA-MPPT controller provides superior and efficient steady-state performance when compared to the PSO-MPPT controller.

Performance of proposed controller is analysed by comparing its efficiency with its competitive controllers mentioned above (η), which can be calculated by

$$\eta = \frac{P_1}{P_2} \times 100\%, \tag{13}$$

where P_1 is the steady-state output power and P_2 is the maximum power output of PV system under particular PSC. Comparison chart of tracking efficiency is shown in Figure 12.

The steady-state performance of both algorithms can be analysed from Figure 11. It is clear that the proposed SMA-MPPT algorithm has better steady-state performance comparing with PSO since the duty cycle of the SMA-MPPT controller oscillates significantly less than the duty cycle of the PSO-MPPT controller, which oscillates more. Additionally, based on Figures 8 and 9, the suggested method executes in 0.51 s and 0.53 s, respectively, for V and I at GMPP. According to simulation results in MATLAB, the MPPT efficiency of the proposed controller for NUC-1 and NUC-2 is 99.89 and 99.81, respectively, which is greater than the efficiency of PSO, which is 98.87 and 98.96 for NUC-1 and NUC-2, respectively. The suggested algorithm also offers a faster tracking speed and a better steady-state oscillation-free response.

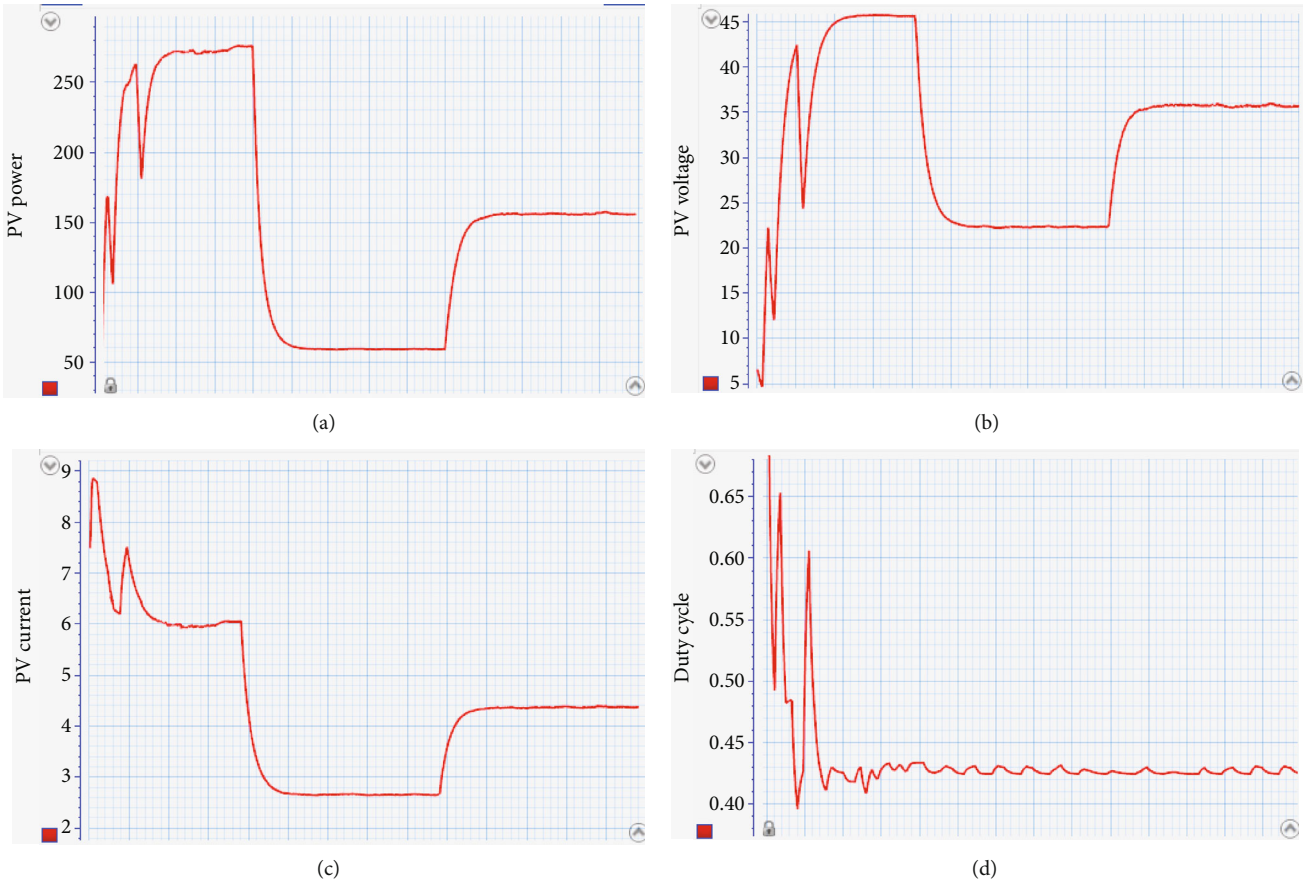

Figure 14: Experimental setup results in ControlDesk: (a) PV power, (b) PV voltage, (c) PV current, and (d) duty cycle.

Table 4: Comparison of performance between the proposed MPPT method and other methods.

Algorithm	Tracking accuracy	Tracking speed	Convergence to GP	Steady-state oscillations	Power efficiency
PO	Low	Slow	Possible to occur in LP	Yes	Low
PSO	Medium	Moderate	Yes	No	Medium
SMA	High	Fast	Yes	No	High

5. Experimental Results

The controller is developed using dSPACE MicroLabBox and RTI1202 to assess the viability and effectiveness of the suggested SMA-MPPT algorithm. MicroLabBox is an all-in-one prototyping unit development system. The tremendous computation power and quick input/output times of MicroLabBox make it one of the system's main advantages. It has an FPGA that can be programmed. Real-time interface (RTI) for Simulink and ControlDesk, which offers simple access to the real-time applications during run time with the use of graphical tools, are two comprehensive dSPACE software packages used in the hardware-in-loop simulation. As illustrated in Figure 13, the effectiveness of the proposed SMA-MPPT algorithm as well as the experimental results under varied irradiance circumstances is evaluated using a hardware-in-loop prototype (HIL) prototype.

Figure 13 shows the total experimental setup of the standalone solar PV system. Additionally, real-time simulation is used to assess the system performance under both UC and NUC situations. The suggested controller is tested using RTS, which uses the model as a HIL prototype. Additionally, ControlDesk software has created a graphical user interface (GUI) for dSPACE MicroLabBox that allows users to alter the PV climate during a simulation's runtime.

Figure 14 illustrates experimental setup results from ControlDesk that demonstrate the proposed SMA-MPPT algorithm's capability to precisely locate and track the GMPP under various PSCs. The standalone solar PV system with the intelligent SMA-MPPT controller has been used in this investigation under three different irradiance situations. In Figure 14, the dynamic waveforms are displayed. The proposed algorithm's PV system shows that the GMPP can be accurately captured and monitored under a variety of solar irradiance circumstances.

Table 5: Experimental results of PO, PSO, and SMA.

Irradiance condition	MPPT method	Voltage (V)	Current (A)	Power (W)	Power efficiency (%)	Tracking time (sec)
			UC (1000 W/m^2)			
V_{mpp} = 45.95 V	PO	41.64	6.31	262.75	97.0	1.52
I_{mpp} = 5.88 A	PSO	43.90	6.04	265.18	97.9	0.76
P_{mpp} = 270.60 W	SMA	45.76	5.86	268.16	99.1	0.53
			NUC-1 (300, 400, 200, and 500 W/m^2)			
V_{mpp} = 23.33 V	PO	23.79	2.52	59.97	96.4	1.20
I_{mpp} = 2.66A	PSO	25.29	2.41	60.97	98.1	0.25
P_{mpp} = 62.15 W	SMA	25.63	2.42	62.03	99.8	0.24
			NUC-2 (500, 800, 700, and 800 W/m^2)			
V_{mpp} = 35.44 V	PO	31.13	4.67	145.42	97.0	1.10
I_{mpp} = 4.23A	PSO	34.88	4.25	148.26	98.8	0.21
P_{mpp} = 149.91 W	SMA	35.18	4.24	149.16	99.4	0.21

The performance comparison of PO, PSO, and the proposed SMA-MPPT method is given in Table 4. Experimental results are given in Table 5. The proposed SMA-MPPT method can track global MPP with high accuracy, very high tracking speed, and high power efficiency with no steady-state oscillations.

6. Conclusion

In this study, a novel MPPT controller based on a slime mould optimization technique is presented. It suppresses some intrinsic issues that most commonly employed MPPT algorithms have. The algorithm's primary work is to initialise the SMA parameters before randomly assigning duty cycle values to each member of the population. Once the best duty cycle is identified for a favourable P-V curve position, the parameters are tuned based on weights to track the best duty cycle for generating MPP under dynamic irradiance conditions. A notion of weight is developed for each individual to counter the potential for capitulating to LMPP. The effectiveness of the proposed MPPT controller is substantiated in MATLAB and validated by hardware implementation. To prove the SMA-MPPT controller's superiority, its performance is compared to that of other cutting-edge approaches (PSO and PO), which proves the eminence of the SMA-MPPT controller.

Data Availability

The data used to support the findings of this study are included in the article.

Conflicts of Interest

The authors declare that they have no conflicts of interest to this work.

References

[1] V. Saxena, N. Kumar, B. Singh, and B. Panigrahi, "A rapid circle centre-line concept-based MPPT algorithm for solar photovoltaic energy conversion systems," *IEEE Transactions on Circuits and Systems I: Regular Papers*, vol. 68, pp. 1–10, 2020.

[2] S. Uprety and H. Lee, "A 0.65-mW-to-1-W photovoltaic energy harvester with irradiance-aware auto-configurable hybrid MPPT achieving >95% MPPT efficiency and 2.9-ms FOCV transient time," *IEEE Journal of Solid-State Circuits*, vol. 56, pp. 1–1, 2020.

[3] A. D. Dhass, N. Beemkumar, S. Harikrishnan, and H. M. Ali, "A review on factors influencing the mismatch losses in solar photovoltaic system," *International Journal of Photoenergy*, vol. 2022, Article ID 2986004, 27 pages, 2022.

[4] K. Padmanaban and A. Shunmugalatha, "Fibonacci based fuzzy controller for grid connected solar photovoltaic system," *Solid State Technology*, vol. 64, no. 2, pp. 2164–2175, 2021.

[5] H. Li, D. Yang, W. Su, J. Lu, and X. Yu, "An adaptive SOM neural network method to distributed formation control of a group of AUVs," *IEEE Transactions on Industrial Electronics.*, vol. 15, pp. 1–1, 2018.

[6] J. P. Ram, D. S. Pillai, N. Rajasekar, and S. M. Strachan, "Detection and identification of global maximum power point operation in solar PV applications using a hybrid ELPSO-P&O tracking technique," *IEEE Journal of Emerging and Selected Topics in Power Electronics*, vol. 8, pp. 1–1, 2019.

[7] A. Ali, K. Almutairi, P. Sanjeevikumar et al., "Investigation of MPPT techniques under uniform and non-uniform solar irradiation condition - a retrospection," *IEEE Access*, vol. 8, pp. 127368–127392, 2020.

[8] A. Gupta, Y. Chauhan, and T. Maity, "A new gamma scaling maximum power point tracking method for solar photovoltaic panel feeding energy storage system," *IETE Journal of Research*, vol. 67, no. 1, pp. 15–35, 2021.

[9] S. Revathy, V. Kirubakaran, M. Rajeshwaran et al., "Design and analysis of ANFIS – based MPPT method for solar photovoltaic applications," *International Journal of Photoenergy*, vol. 2022, Article ID 9625564, 9 pages, 2022.

[10] R. Bollipo, S. Mikkili, and P. Bonthagorla, "Critical review on PV MPPT techniques: classical, intelligent and optimisation," *IET Renewable Power Generation*, vol. 14, no. 9, pp. 1433–1452, 2020.

[11] H. Kraiem, F. Aymen, L. Yahya, A. Triviño, M. Alharthi, and S. S. M. Ghoneim, "A comparison between particle swarm and grey wolf optimization algorithms for improving the battery autonomy in a photovoltaic system," *Applied Sciences (Switzerland)*, vol. 11, no. 16, p. 7732, 2021.

[12] J. Ahmed and Z. Salam, "A maximum power point tracking (MPPT) for PV system using cuckoo search with partial shading capability," *Applied Energy*, vol. 119, pp. 118–130, 2014.

[13] S. Titri, C. Larbes, K. Y. Toumi, and K. Benatchba, "A new MPPT controller based on the ant colony optimization algorithm for photovoltaic systems under partial shading conditions," *Applied Soft Computing*, vol. 58, pp. 465–479, 2017.

[14] M. Seyedmahmoudian, B. Horan, K. S. Tey et al., "State of the art artificial intelligence-based MPPT techniques for mitigating partial shading effects on PV systems–a review," *Renewable and Sustainable Energy Reviews*, vol. 64, pp. 435–455, 2016.

[15] S. Mohanty, B. Subudhi, and P. K. Ray, "A new MPPT design using grey wolf optimization technique for photovoltaic system under partial shading conditions," *IEEE Transactions on Sustainable Energy*, vol. 7, no. 1, pp. 181–188, 2016.

[16] A. s. Benyoucef, A. Chouder, K. Kara, S. Silvestre, and O. A. sahed, "Artificial bee colony based algorithm for maximum power point tracking (MPPT) for PV systems operating under partial shaded conditions," *Applied Soft Computing*, vol. 32, pp. 38–48, 2015.

[17] A. Mirza, M. Mansoor, Q. Ling, B. Yin, and M. Y. Javed, "A salp-swarm optimization based MPPT technique for harvesting maximum energy from PV systems under partial shading conditions," *Energy Conversion and Management*, vol. 209, article 112625, 2020.

[18] S. Li, H. Chen, M. Wang, A. A. Heidari, and S. Mirjalili, "Slime mould algorithm: a new method for stochastic optimization," *Future Generation Computer Systems*, vol. 111, pp. 300–323, 2020.

[19] H. M. Ridha, C. Gomes, H. Hizam, M. Ahmadipour, A. A. Heidari, and H. Chen, "Multi-objective optimization and multi-criteria decision-making methods for optimal design of standalone photovoltaic system: a comprehensive review," *Renewable and Sustainable Energy Reviews*, vol. 135, article 110202, 2021.

[20] S. Sivakumar, M. J. Sathik, P. S. Manoj, and G. Sundararajan, "An assessment on performance of DC-DC converters for renewable energy applications," *Renewable and Sustainable Energy Reviews*, vol. 58, pp. 1475–1485, 2016.

[21] S. Dorji, D. Wangchuk, T. Choden, and T. Tshewang, "Maximum power point tracking of solar photovoltaic cell using perturb & observe and fuzzy logic controller algorithm for boost converter and quadratic boost converter," *Materials Today: Proceedings*, vol. 27, pp. 1224–1229, 2020.

[22] K. Atici, I. Sefa, and N. Altin, "Grey wolf optimization based MPPT algorithm for solar PV system with SEPIC converter," in *2019 4th International Conference on Power Electronics and their Applications (ICPEA)*, vol. 1, pp. 1–6, Elazig, Turkey, 2019.

[23] A. Raj, S. R. Arya, and J. Gupta, "Solar PV array-based DC-DC converter with MPPT for low power applications," *Renewable Energy Focus*, vol. 34, pp. 109–119, 2020.

[24] R. Durga Devi and S. Nageswari, "Distributed SM MPPT controller for solar PV system under non-uniform atmospheric conditions," *IETE Journal of Research*, vol. 66, pp. 1–10, 2020.

[25] M. A. Farahat, H. M. B. Metwally, and A. Abd-Elfatah Mohamed, "Optimal choice and design of different topologies of DC-DC converter used in PV systems, at different climatic conditions in Egypt," *Renewable Energy*, vol. 43, no. 3, pp. 393–402, 2012.

[26] M. H. Taghvaee, M. A. M. Radzi, S. M. Moosavain, H. Hizam, and M. HamiruceMarhaban, "A current and future study on non-isolated DC-DC converters for photovoltaic applications," *Renewable and Sustainable Energy Reviews*, vol. 17, pp. 216–227, 2013.